NJC

ROYAL SOCIETY OF CHEMISTRY

PAPER

View Article Online
View Journal | View Issue

Cite this: *New J. Chem.*, 2021, 45, 15869

A xanthene-based novel colorimetric and fluorometric chemosensor for the detection of hydrazine and its application in the bio-imaging of live cells†

Uday Narayan Guria,[a] Saikat Kumar Manna,[b] Kalipada Maiti,[c] Sandip Kumar Samanta,[a] Aritri Ghosh,[d] Pallab Datta,[d] Debasish Mandal[e] and Ajit Kumar Mahapatra *[a]

Received 15th June 2021,
Accepted 28th July 2021

DOI: 10.1039/d1nj02943f

rsc.li/njc

Efficient reactive fluorescent chemosensors are generating considerable attention for analyte detection due to easy instrumentation, low cost and quick response. Hydrazine is a reactive chemical substance to the industry and is toxic to human health. Herein, an ICT-based hydrazine-responsive chemodosimeter 2-{(7,8-dihydro-3-methoxy-6*H*-xanthen-5-yl)methylene}-2*H*-indene-1,3-dione (**MXI**) sensor with high selectivity and quick response has been designed, synthesized and characterized. Upon treatment with hydrazine, the probe displays a distinct colour change to the naked eye, from violet to colourless in DMSO aqueous solution and a turn-on fluorescent signal is achieved. DFT calculations reveal that the hypsochromic shift in absorbance spectra and fluorescent enhancement was due to ICT (intramolecular charge transfer) blocking upon reaction with hydrazine and the probe. By its successful demonstrations in real-time test kit sensing, this probe overcomes most of the drawbacks of the fluorescent probes of recent times. Furthermore, this probe has also been effectively utilized for imaging intracellular hydrazine in human bone osteosarcoma (MG63) cells.

Introduction

Hydrazine is a colourless, volatile, flammable and highly reactive liquid compound that is extensively employed in many areas including chemical, pharmaceutical, agriculture and food industries.[1–8] In addition, hydrazine serves not just as an efficient reagent in a variety of organic synthesis (*e.g.*, Wolff–Kishner reduction), but also as the most commonly used propellant in rockets, missiles, space-shuttle and satellites due to its detonable nature, hypergolic characteristics and the high enthalpy of combustion.[9–11] Furthermore, it has been reported that certain nitrogen-fixing bacteria, anammox organisms and yeasts generate hydrazine as a by-product of natural biochemical processes.[12] Recently, various hydrazine derivatives including hydralazine, isoniazid and isocarboxazide are employed in the treatment of heart disease and hypertension.[13] In spite of its important function, water-soluble hydrazine is extremely toxic to human health and animals as it is rapidly ingested by inhalation, dermal and oral intake, associated with significant deterioration to the body parts (kidneys, lungs, liver), central nervous system, respiratory tract and spleen.[14–17] Moreover, long-term exposure to these harmful chemicals can lead to adverse effects on proteins and DNA.[18–22]

Thus, World Health Organization and U.S. Environmental Protection Agency (EPA) have listed hydrazine as a potential carcinogen and also proposed its threshold value in drinking water as 10 ppb.[23,24] The design and development of an effective method for the determination of hydrazine in environmental and biological systems are therefore of major concern. Thus far, numerous traditional analytical and spectroscopic techniques have been utilized for the qualitative/quantitative estimation of hydrazine, such as HPLC (high-performance liquid chromatography),[25] gas chromatography,[26] ion chromatography,[27] titrimetry,[28,29] electrochemical methods,[30–33] and surface-enhanced

[a] *Department of Chemistry, Indian Institute of Engineering Science and Technology, Shibpur, Howrah-711103, West Bengal, India. E-mail: akmahapatra@rediffmail.com; Fax: +913326684564*
[b] *Department of Chemistry, Haldia Government College, Debhog, Purba Medinipur, West Bengal-721657, India*
[c] *Department of Chemistry, University of Calcutta, University College of Science, 92, A. P. C. Road, Kolkata 700009, India*
[d] *Centre for Healthcare Science, Indian Institute of Engineering Science and Technology, Shibpur, Howrah 711103, India*
[e] *School of Chemistry and Biochemistry, Thapar Institute of Engineering and Technology, Patiala 147004, Punjab, India*

† Electronic supplementary information (ESI) available. CCDC 2069443. For ESI and crystallographic data in CIF or other electronic format see DOI: 10.1039/d1nj02943f

Raman spectroscopy (SERS),[34] but these approaches are costly, time-consuming, complicated and not convenient for frequent use and detection in biological specimens. Compared to these common procedures, the fluorogenic/chromogenic techniques of the spectral area are much more suitable owing to their easiness, high selectivity, high sensitivity, accuracy, quick response, reasonable cost, real-time detection, non-destructive nature and capability of imaging living systems.[35] To date, many fluorescent probes have been utilized to detect hydrazine and most of them sense hydrazine *via* several sensing strategies, such as (i) deprotection[36] (ii) nucleophilic addition–elimination on keto ester[37–39] (iii) cyclization (iv) group transformation (v) Gabriel amine synthesis (vi) hydrogen bonding-based design and (vii) other approaches.[40–44] Beside this, there are still a few shortcomings with the reported probes, including low water solubility, ineffective detection limits, poor fluorescence signal, long reaction time, minor stoke shifts, high background signal and limited practical applications.

In view of all of the above disadvantages in our mind, herein, we have constructed an ICT-based chemodosimeter **MXI** comprising of a 1,3-indanedione acceptor and a xanthene donor for the highly selective and sensitive detection of hydrazine *via* the hydrazone formation reaction strategy. We anticipated that in the presence of hydrazine, a unique reaction between 1,3-indanedione moiety and hydrazine produced fluorescent hydrazone, which disrupted the intramolecular electron density distribution, leading to the fluorometric and colorimetric changes in DMSO–H_2O (10 mM HEPES buffer, 3 : 7 v/v, pH 7.4, at 25 °C). The probe **MXI** displayed a fast fluorescence response to hydrazine within 3 minutes and a noticeable fluorescence enhancement at 519 nm along with a large blue shift of 177 nm in the absorption band in the presence of hydrazine. This chemodosimeter provides excellent adequacy over some reported chemodosimeters in terms of a simple synthetic route with good yield, dual-sensing techniques (fluorometric and colorimetric), selectivity and sensitivity. Nucleophilic addition followed by retro-aldol reaction of hydrazine on dicyano malononitrile acceptor to yield hydrazone derivative remained a common strategy in hydrazine detection.[45] Here in our study, we have introduced a 1,3-indanedione acceptor as a reactive unit instead of malononitrile for hydrazine detection. Moreover, our probe **MXI** can also be used in hydrazine detection in living human bone osteosarcoma (MG63) cells.

Results and discussions

The probe **MXI** was synthesized *via* a multistep reaction from a commercially available cyclohexanone molecule, as shown in Scheme 1. The chemical structure of **MXI** was fully characterized by ^{1}H NMR, ^{13}C NMR and mass spectroscopy. In addition, the chemical structure of compound **2** was also confirmed by single-crystal X-ray diffraction analysis (ESI,† Deposition Number 2069443).

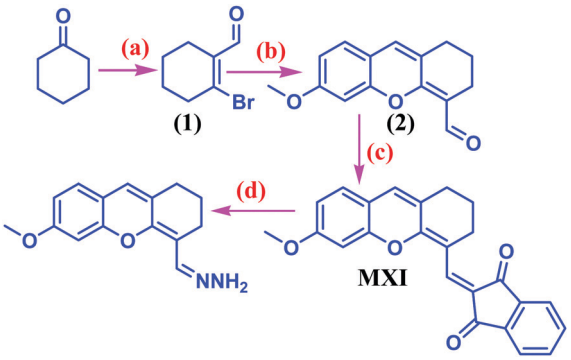

Scheme 1 Synthetic schemes for probe **MXI**: (a) DMF, PBr_3, $CHCl_3$, addition at 0 °C then stirred at room temperature for 16 h. (b) 2-hydroxy-4-methoxybenzaldehyde, Cs_2CO_3, DMF, 25 °C, 16 h. (c) 1,3-Indandione, dry EtOH, piperidine, reflux for 8 h. (d) DMSO, NH_2NH_2.

Colorimetric and fluorometric response towards N_2H_4

The photophysical properties (absorption and emission) of chemodosimeter **MXI** in the absence and presence of hydrazine were measured in DMSO–H_2O (10 mM HEPES buffer, 2 : 8 v/v, pH 7.4, at 25 °C). Initially, the absorption spectra of chemodosimeter **MXI** revealed a broad ICT band centred at 568 nm. However, upon gradual addition of hydrazine (20 equiv.) to the organo-aqueous solution of **MXI**, a new absorption band was formed at 391 nm with a concomitant decrease of the original absorption peak at 568 nm.

The existence of an isosbestic point at 452 nm indicates the formation of a new compound in the reaction mixture due to chemodosimetric reaction between **MXI** and hydrazine. Such a strong blue shift of 177 nm in the absorption spectra results in the change in color of the solution from violet to colorless. Probe **MXI** can therefore act as a ''naked-eye'' sensor for hydrazine. The absorption intensity ratios at 568 nm and 391 nm ($A_{568\,nm}/A_{391\,nm}$) linearly increased with the concentration of hydrazine ranging from (0.5–25 μM) (Fig. S8, ESI†) and the limit of detection was estimated to be 75 nM. Moreover, other competitive analytes did not demonstrate any substantial changes in the absorption spectra, indicating excellent selectivity of **MXI** for hydrazine (Fig. 1b). The free probe **MXI** displayed a weak emission band centred at 498 nm upon excitation at 452 nm, as shown in Fig. 2a. Meanwhile, the addition of hydrazine (2 equiv.) to the probe solution resulted in a large increase in the fluorescence intensity at 519 nm with a small red shift. In this context, fluorescence color of the solution changes from dark to green. In order to analyze the selectivity of the chemodosimeter **MXI**, the fluorescence response to different analytes (CO_3^{2-}, SO_4^{2-}, HPO_4^{2-}, AcO^-, NO_3^-, N_3^-, N_2H_4, I^-, Br^-, Cl^-, Cys, Lys, GSH and His) were evaluated. Upon the addition of hydrazine to the solution of **MXI**, only hydrazine generated a significant increase in emission intensity at 519 nm, while others analytes (10 equiv.) did not cause any noticeable changes on the emission spectra of **MXI**. In addition, competitive studies were conducted upon the addition of hydrazine to the probe's solution in the presence of 50 equivalents of different analytes (anions and amino acids). It was noticed that the fluorescence enhancement by hydrazine was

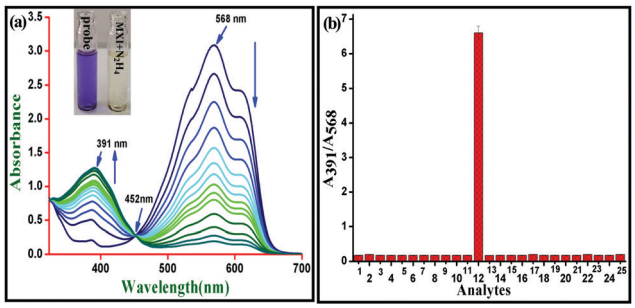

Fig. 1 (a) Absorption spectra of **MXI** (10 μM) upon addition of hydrazine (2 equiv.) in DMSO–H_2O (10 mM HEPES buffer, 3 : 7 v/v, pH 7.4, at 25 °C). Inset: Visible photographic images of **MXI** and **MXI** + hydrazine. (b) Selectivity bar diagram of **MXI** upon addition of different analytes (1. CO_3^{2-}, 2. SO_4^{2-}, 3. HPO_4^{2-}, 4. AcO^-, 5. NO_3^-, 6. N_3^-, 7. I^-, 8. DIPEA, 9. phenol, 10. TEA, 11. urea, 12. N_2H_4, 13. PhSH, 14. $PhNH_2$, 15. Thiourea, 16. Br^-, 17. Cl^-, 18. Cys, 19. Lys, 20. GSH, 21. His, 22. Zn^{2+}, 23. Cr^{3+}, 24. Na^+, 25. Cu^{2+}) in DMSO–H_2O (10 mM HEPES buffer, 3 : 7 v/v, pH 7.4, at 25 °C) including error bars (error amount, 5%; Y error bar for both [±] deviations).

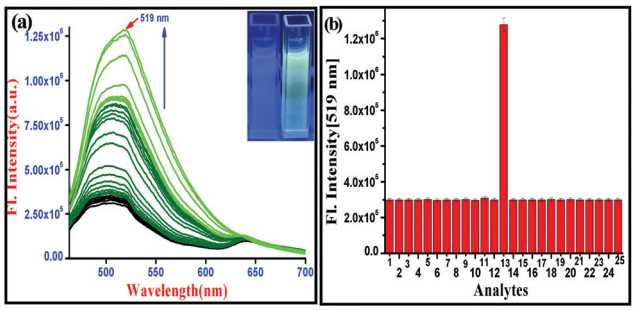

Fig. 2 (a) Fluorescence spectra of **MXI** (10 μM) at λ_{ex} = 452 nm, upon addition of hydrazine (2 equiv.) in DMSO–H_2O (10 mM HEPES buffer, 3 : 7 v/v, pH 7.4, at 25 °C. (b) Fluorescence selectivity bar diagram of **MXI** upon the addition of different analytes [1. CO_3^{2-}, 2. SO_4^{2-}, 3. HPO_4^{2-}, 4. AcO^-, 5. NO_3^-, 6. N_3^-, 7. I^-, 8. DIPEA, 9. phenol, 10. TEA, 11. urea, 12. PhSH, 13. N_2H_4, 14. $PhNH_2$, 15. Thiourea, 16. Br^-, 17. Cl^-, 18. Cys, 19. Lys, 20. GSH, 21. His, 22. Zn^{2+}, 23. Cr^{3+}, 24. Na^+, 25. Cu^{2+} (10.0 equiv. of each)] in DMSO–H_2O (10 mM HEPES buffer, 3 : 7 v/v, pH 7.4, at 25 °C), including error bars (error amount, 5%; Y error bar for both [±] deviations).

not influenced by the presence of other competitive analytes (Fig. S7, S14 and S15, ESI†), suggesting that the probe **MXI** is extremely specific to hydrazine.

Then, the detection ability of **MXI** (10 μM) to hydrazine at different pH was evaluated. As depicted in Fig. S13 (ESI†), the probe **MXI** is reluctant to respond at a different pH range from 0–14. Again, in the presence of hydrazine no such pH-responsive fluorescent change was observed within the given pH range (0–14). Thus, **MXI** is able to sense hydrazine in a wide range of pH, which delivers a basis for its application in biology.[46]

Sensing mechanism

The probable sensing mechanism of chemodosimeter **MXI** for hydrazine is shown in Scheme 2. The chemodosimetric probe **MXI** is weakly fluorescent, most probably due to the electron

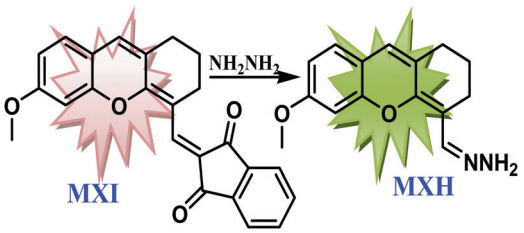

Scheme 2 Probable sensing mode of **MXI**.

transfer between the methoxy group of xanthenes to indandione moieties through the donor–acceptor system.[47] Upon reaction with hydrazine *via* the Michael reaction pathway, probe **MXI** releases the fluorescent quencher indandione moiety to produce hydrazone of **MXH**, which exhibits a strong fluorescent change. The above fluorogenic and chromogenic response of **MXI** towards hydrazine was mostly attributed to the formation of hydrazone (**MXH**). This hydrazine-induced chemodosimetric reaction deactivates the ICT process, leading to a 177 nm hypsochromic shift in the absorption bands and a green fluorescence at 519 nm. To validate the sensing process HRMS (high-resolution mass spectroscopy) analysis was carried out (Fig. S6, ESI†). As shown in Fig. S3 (ESI†), the free probe (**MXI**) exhibits a distinct peak at m/z = 371.1269 (calculated = 370.1205).

Whereas, upon the addition of 2 equivalent of hydrazine to the solution of **MXI**, a new peak is generated at m/z = 257.1308 (calc. = 257.1212), revealing the formation of hydrazone 1-[(7,8-dihydro-3-methoxy-6*H*-xanthen-5-yl)methylene]hydrazone (**MXH**) (Fig. S6, ESI†). In addition, the progress of the reaction was monitored by TLC (thin layer chromatography) (Fig. S9, ESI†). We have checked the ability of compound **2** for hydrazone formation with hydrazine and studied the reaction, but find that the reaction was occurring.

The response rate of MXI to hydrazine

For reactive chemical sensor reaction kinetics is a proficient parameter for real-time application of the probe. In this context, time-dependent fluorescence measurement was measured to evaluate the reaction time required between the probe **MXI** and hydrazine.

From Fig. 3b, it was observed that the time needed for the fluorescence intensity (519 nm) to reach the plateau was about 3.0 min. From the kinetic profile of the probe **MXI** (10 μM) with NH_2NH_2(>20 equiv.), a pseudo-first-order rate constant of 0.00567 S^{-1} was found (Fig. 3a)

Density functional theory (DFT) calculations

In order to better understand the sensing process, we implemented density functional theory (DFT) calculations using the B3LYP/6-311+G(d,p) basis set of the Gaussian 09 program. The structures of the probe **MXI** and product MXH were optimized and their highest occupied molecular orbital (HOMO) and the lowest unoccupied molecular orbital (LUMO) were also determined (listed in Table S2 (ESI†)).

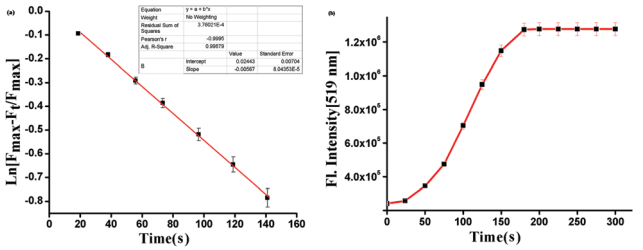

Fig. 3 (a) Pseudo first-order kinetic profile of **MXI** (10 μM) upon the addition of N_2H_4 (20 equiv.) in DMSO–H_2O (10 mM HEPES buffer, 3 : 7 v/v, pH 7.4, at 25 °C). Including error bars (error amount, 5%; Y error bar for both [±] deviations). (b) Time-dependent fluorescence response of **MXI** (10 μM, in DMSO–H_2O) upon the addition of N_2H_4 (2 equiv.) including error bars (error amount, 3%; Y error bar for both [±] deviations).

As presented in Fig. 4, electrons were primarily distributed on the xanthene moiety in HOMO and shifted to the 1,3-indanedione acceptor part in LUMO, suggesting a higher ICT effect. Moreover, the HOMO–LUMO energy gap (3.04 eV) of the hydrazone (**MXH**) was greater than that of the free probe **MXI** (2.36 eV) and this significantly correlates with the experimental results.

The electronic structural properties of the ground state and the excited state of **MXI** were calculated based on single-excitation time-dependent DFT (TDDFT). Fundamental electronic transitions calculated by TDDFT (Table S1, ESI†) were analogous to the experimentally observed absorbance spectra. The studies suggest that the vertical major transitions (HOMO–LUMO, f = 1.2242, ΔE = 2.36 eV) observed at ~524 nm are comparable to those with experimentally observed spectra at ~568 nm for **MXI**. Whereas, HOMO–LUMO (f = 0.7029, ΔE = 3.04 eV) observed at 407.68 nm is comparable with the experimental peak at 391 nm for MXH.

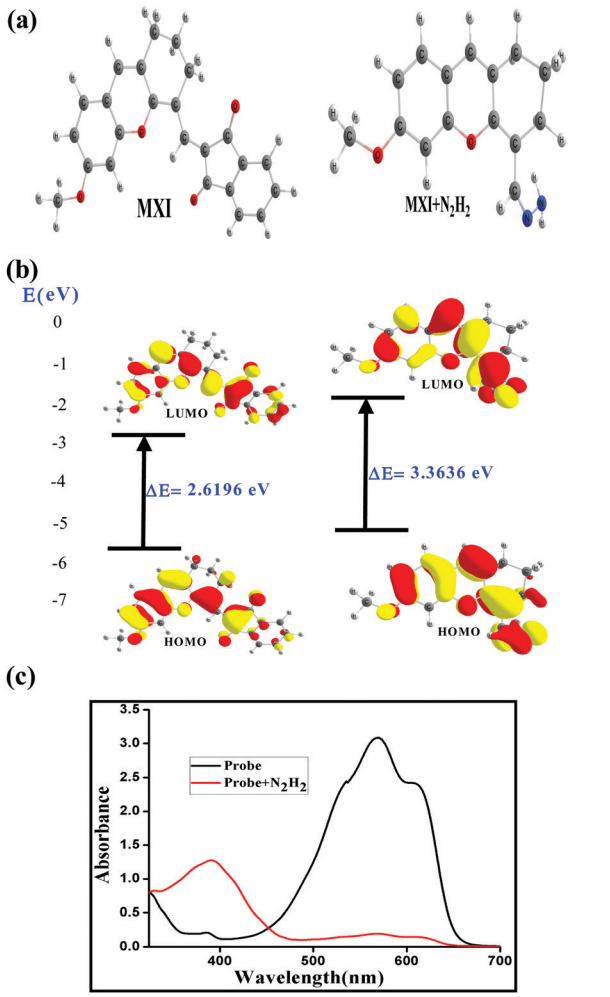

Fig. 4 Quantum chemical calculation of **MXI** and its reaction product. (a) The most stable conformational structures of **MXI** and its reaction product (**MXI** + N_2H_4). (b) HOMO/LUMO and their energy difference (ΔE, unit: eV) of **MXI** and product (**MXI** + N_2H_4) obtained by DFT calculations (TDDFT//B3LYP/6-311+G(d,p)). (c) Calculated electronic absorption spectra of **MXI** and product (**MXI** + N_2H_4) in water/DMSO.

Practical application

The intense color change of the probe **MXI** in solution recommends as an excellent test kit sensor for hydrazine. For this purpose, test strips were prepared by dipping the filter paper into the acetonitrile solution of **MXI** (c = 1.0 × 10^{-3} M) and then exposed to air for drying. **MXI** immersed filter plates were treated with various concentrations of hydrazine and a noticeable color change was observed from deep violet to colorless as seen by the naked eye (Fig. 5). Also, a dramatic fluorescence change in strips was observed from blue to green upon treatment with various concentrations of hydrazine. These results suggest that the probe would be used as a hydrazine responsive device for real-time applications.

Cell imaging study

The selectivity and sensitivity of **MXI** towards NH_2NH_2 were examined in live osteosarcoma cell line MG63. The compound was incubated with cells in different volumes (2, 5, 7.5, 10, 15 μL) to assess the cellular uptake of **MXI** and cellular viability towards **MXI** alone for 1 hour. Further, the **MXI**-treated MG63 cells were also assessed for cellular viability after the treatment with NH_2NH_2 for 1 hour. The cellular viability of MG63 cells was assessed after both treatments with **MXI**, with or without

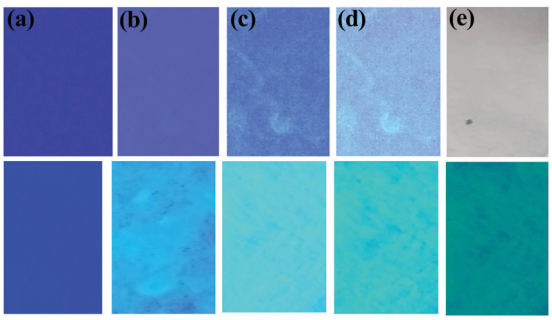

Fig. 5 Photographs of **MXI**/filter papers upon exposure to hydrazine in the presence daylight (top) and fluorescent light (bottom). (a) **MXI** (1.0 × 10^{-4} M), (b) 10.0 × 10^{-4} M N_2H_4, (c) 25.0 × 10^{-4} M N_2H_4, (d) 40.0 × 10^{-4} M N_2H_4, (e) 80.0 × 10^{-4}M N_2H_4.

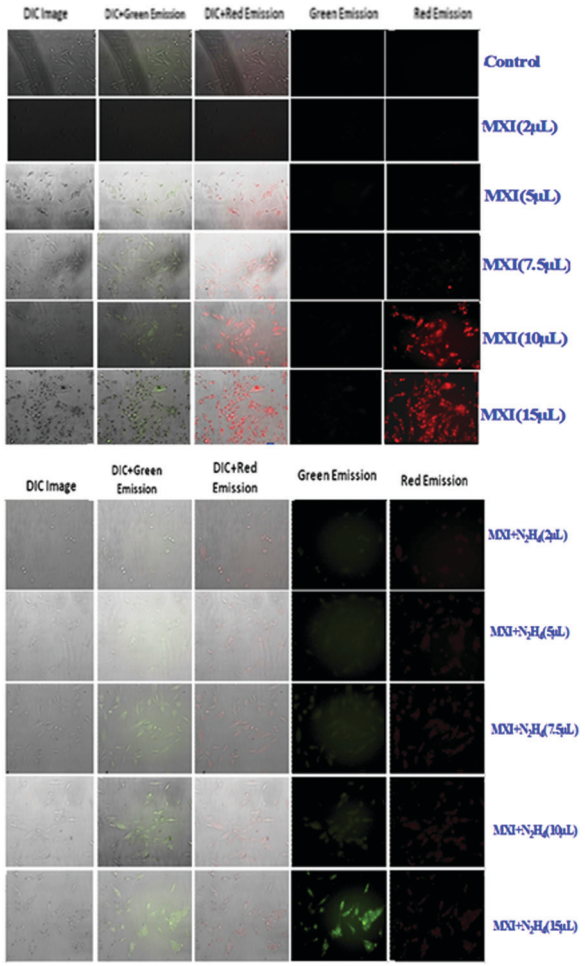

Fig. 6 Fluorescence microscopy images of **MXI** in osteosarcoma cell line MG63. (Top) Live cells treated with only **MXI** at different volumes, (bottom) live cells treated with **MXI** and hydrazine.

secondary treatment with NH_2NH_2 and represented in Fig. S10 (ESI†). The Mg 63 cells showed 73.51% ± 0.95, 65.87% ±0.5, 52.98% ± 1.05, 44.4% ± 1.19 and 32.9% ± 0.85 corresponding to 2, 5, 7.5, 10 and 15 μL of **MXI** alone respectively. Subsequent incubation with NH_2NH_2 showed a slight decrease in cellular viability to 61.216% ± 1.92, 56.77% ± 1.41, 54.67% ± 2.61, 41.32% ± 1.25 and 31.32% ± 2.25 corresponding to 2, 5, 7.5, 10 and 15 μL of NH_2NH_2, respectively. The lowering of cellular viability stops with the increase in NH_2NH_2 and **MXI** volumes and is indicative of their reactive nature.

The MG63 cells, which have up-taken **MXI** were imaged by fluorescence microscopy by exciting in the green (512–552 nm with a bandwidth of 40 nm) region and with emission wavelengths between 565–615 nm (red emission) with a bandwidth of 50 nm.

The cells showed a very weak red emission with an increase in the volume of **MXI** treatment. When the cells were incubated with **MXI** and subsequently followed by NH_2NH_2 a strong increase in the emission fluorescence in the green region (ex: 465–495 nm (blue region) with bandwidth 30 nm, em: 515–555 nm (green emission) with bandwidth of 40 nm) was observed and the red emission diminished correspondingly with the increase in NH_2NH_2 volume. The reason for these changes from red to green emission might be attributed to the formation of hydrazone in MG63 live cells. The images for the fluorescence emissions are represented in Fig. 6.

Conclusion

In summary, we have devised and synthesized a new ICT-based fluorogenic and ratiometric chromogenic chemodosimeter **MXI** for the detection of hydrazine *via a* hydrazone formation strategy. The sensing mechanism between **MXI** and hydrazine has been extensively discussed by absorption and emission spectra, HRMS and DFT calculations. The emission response of **MXI** toward hydrazine is very fast (within 3 min), which confirms that the probe **MXI** may sense hydrazine in real time. From the UV-vis titration data, the limit of detection was estimated to be 75 nM. Especially, the change in optical properties of **MXI** in the presence of hydrazine is extremely selective, because various comparative analytes cannot interfere with hydrazone-forming reactions. Furthermore, cell imaging experiments indicated that the probe **MXI** could be employed to image hydrazine in living human bone osteosarcoma (MG63) cells. We assume that our chemodosimeter can provide an efficient technique for the detection of hydrazine in the solution phase as well as in biological systems.

Experimental section

Materials and methods

Unless otherwise mentioned, materials were obtained from commercial suppliers and were used without further purification. ^1H and ^{13}C NMR spectra were recorded on Bruker 500 and 100 MHz instruments. For NMR spectra, DMSO-d_6 and $CDCl_3$ were used as solvents using TMS as an internal standard. Chemical shifts are expressed in δ ppm units and ^1H–^1H and ^1H–C coupling constants in Hz. Mass spectra were measured using a Waters QTOF Micro YA 263 mass spectrometer. Fluorescence spectra were recorded on a PerkinElmer Model LS 55 spectrophotometer. UV spectra were recorded on a JASCO V-530 spectrophotometer.

Cell imaging study

MG63 (human bone osteosarcoma obtained from NCCS, Pune) cells were cultured in DMEM high glucose (Gibco-REF12800-058) medium with 10% HI-FBS (GibcoREF16140-063) and 1% antibiotic and antimycotic (Gibco-REF 25200-072) solution at 37 °C and 5% CO_2 in a humidified incubator (Esco-AC2-4S8). Upon reaching 70–80% confluency, MG63 cells were harvested using 0.05% Trypsin-EDTA (Gibco-REF25200-072) and used for cellular viability and imaging studies. Then, the culture plates were placed into a humidified atmosphere of 95% air and 5% CO_2 at 37 °C for more than 2 hours, for cellular attachment. Then, the unattached cells were washed with 1XPBS and fresh cell culture medium was added and plates were kept in a

humidified incubator until the cell layer reached 80–90% confluency.

After the cell layer reached the desired confluency, the cell layer was washed with 1 × PBS, and replenished with different concentrations (2, 5, 7.5, 10 and 15 μL) of **MXI** with incomplete media and incubated for 1 hour. After 1 hour, the media with **MXI** was removed and different concentrations of NH_2NH_2 (2, 5, 7.5, 10 and 15 μL) in incomplete media were added to the cells for another hour of incubation. Following this treatment, the treated cells were used for studying cellular viability and microscopic image acquisition.

Cytotoxic effect on cells

The cellular viability of the **MXI**-NH_2NH_2 treated cells was studied by MTT assay (Himedia-CCK003) by following the standard protocol. MG63 cells were seeded onto 96-well plates (approximately 10^4 cells per well) and cultured for 24 hours. The next day, the media was discarded and various concentrations of **MXI** and NH_2NH_2 made in DMEM were added to the cells and incubated as per the protocol mentioned previously. Cells treated with the only medium were positive control and DMSO served as a negative control. Following incubation, the growth media was removed, and fresh incomplete DMEM-containing MTT solution was added. Subsequently, the supernatant was removed, the insoluble coloured formazan product was solubilized in DMSO, and its absorbance was measured in a microtiter plate reader (Thermo) at 570 nm and a reference wavelength of 670 nm. Cell viability was quantified by measuring the absorbance at 570 nm and a reference wavelength of 670 nm and cell viability was calculated as a percentage relative to the positive control.

Microscopic image acquisition

For imaging studies, MG63 cells 1 × 10^4 cells per mL of medium were seeded on sterile coverslips and cultured in a 48 well plates and incubated at 37 °C for 24 hours in a humidified CO_2 incubator. After treatment with various concentrations of **MXI** and NH_2NH_2, the coverslips were washed with 1 × PBS thrice and images were acquired using a Nikon inverted microscope (Nikon *EclipseTi*, Japan) under 20x objectives (DIC and S-Plan Fluo) in the following ranges (a) excitation at green region (512–552 nm with a bandwidth of 40 nm), emission at red region (565–615 nm with a bandwidth of 50 nm); (b) excitation at blue region (465–495 nm with bandwidth 30 nm) and emission at green region (515–555 nm with bandwidth of 40 nm).

Computational methods

Geometries have been optimized using the B3LYP/6-31G(d,p) level of theory. The geometries are verified as proper minima by frequency calculations. Time-dependent density functional theory calculation has also been performed at the same level of theory. All calculations have been carried out using the Gaussian 09 program.

Synthesis and structure characterization

Synthesis of the probe

The probe was synthesized *via* a multistep reaction from commercially available cyclohexanone as shown in Scheme 1. The products formed during the synthesis of the probe were purified by column chromatography [Silica gel (100–200 mesh, Merck) was used for column chromatography] and all compounds were fully characterized by HRMS, ^{1}H-NMR, and, ^{13}C-NMR. To a mixture of DMF (11.2 mL) and $CHCl_3$ (50 mL) was added PBr_3 (12.4 mL, 130.5 mmol) dropwise at 0 °C and the mixture was stirred 45 min before adding cyclohexanone (5 mL, 48.4 mmol), the resulting solution was stirred at r.t for 16 h. Then, poured into ice-cold 50 mL water neutralized with $NaHCO_3$ and extracted with DCM, dried over Na_2SO_4, concentrated with a vacuum to give a yellow oil, and used directly in the next step.

Synthesis of 6-methoxy-2,3-dihydro-1*H*-xanthene-4-carbaldehyde (2)

To compound **1** (204 mg, 1.08 mmol) in DMF (6 mL) at 25 °C were added 2-hydroxy-4-methoxybenzaldehyde (137 mg, 0.90 mmol) and Cs_2CO_3 (880 mg, 2.7 mmol). The medium was stirred for 16 h at 25 °C and an intense yellow spot appeared on the TLC plate (hexane: AcOEt = 8 : 2). The insoluble material was then filtered on a pad of silica gel and the filtrate was concentrated. The resulting residue was diluted with dichloromethane (30 mL) and washed with H_2O (2 × 15 mL). The organic layer was dried over Na_2SO_4, filtered, and concentrated using a vacuum. Purification by silica gel column chromatography (CH_2Cl_2: AcOEt = 20 : 1) provided compound **2** as a deep yellow solid (160 mg, 72%). ^{1}H NMR (400 MHz, $CDCl_3$) δ 10.31 (s, 1H), 7.06 (d, J = 4.1 Hz, 1H), 6.65–6.64 (m, 3H), 3.82 (s, 3H), 2.57–2.54 (m, 2H), 2.45 (t, J = 6.2 Hz, 2H), 1.74–1.69 (m, 2H); HR-MS (ESI): m/z calcd for $C_{15}H_{14}O_3^+$ $[M + H]^+$ 243.1016, found 243.1022. Recrystallized with DCM/MeOH mixture.

Synthesis of MXI

Compound **2** (40 mg, 0.16 mmol) and 1,3-indandione (24 mg, 0.16 mmol) was taken in dry EtOH; a catalytic amount of piperidine was added to the mixture. The mixture was refluxed for 8 h, a dark green color precipitate appeared, the solid was filtered and washed with cold ethanol. ^{1}H-NMR (500 MHz, $CDCl_3$) δ 1.83 (m, 2H), 2.16 (m, 2H), 2.66 (m, 2H), 3.8 (s, 3H), 6.73 (s, 1H), 6.85 (m, 1H), 7.16 (m, 1H), 6.91 (s, 1H), 8.44 (s, 1H), 7.86 (d, 2H, J = 3 Hz), 7.68 (d, 2H, J = 2.5 Hz); HR-MS (ESI): m/z calcd for $C_{24}H_{18}O_4^+$ $[M + H]^+$ 371.1205, found 371.1269. ^{13}C-NMR (100 MHz, $CDCl_3$): 24.47, 28.8, 30.1, 56.09, 100.4, 113.09, 113.8, 115.4, 122.2, 122.9, 127.6, 127.9, 129.6(2C), 133.8, 134.2(2C), 139.9(2C), 154.7, 161.01, 162.31, 190.14(2C).

Conflicts of interest

There are no conflicts to declare.

Acknowledgements

We are grateful to CSIR [file no: 02(0334)/18/EME-II] for the financial and research support.

Notes and references

1 U. Ragnarsson, *Chem. Soc. Rev.*, 2001, **30**, 205–213.
2 S. Garrod, M. E. Bollard, A. W. Nicholls, S. C. Connor, J. Connelly, J. K. Nicholson and E. Holmes, *Chem. Res. Toxicol.*, 2005, **18**, 115–122.
3 A. Balsamo, B. Macchia, F. Macchia, A. Rossello, R. Giani, G. Pifferi, M. Pinza and G. Broccali, *J. Med. Chem.*, 1983, **26**, 1648–1650.
4 C. W. Huffman, E. M. Godar, K. Ohki and D. C. Torgeson, *J. Agric. Food Chem.*, 1968, **16**, 1041–1046.
5 W. X. Yin, Z. P. Li, J. K. Zhu and H. Y. Qin, *J. Power Sources*, 2008, **182**, 520–523.
6 S. S. Narayanan and F. Scholz, *Electroanalysis*, 1999, **11**, 465–469.
7 A. Serov, M. Padilla, A. J. Roy, P. Atanassov, T. Sakamoto, K. Asazawa and H. Tanaka, *Angew. Chem.*, 2014, **53**, 10336–10339.
8 K. Yamada, K. Yasuda, N. Fujiwara, Z. Siroma, H. Tanaka, Y. Miyazaki and T. Kobayashi, *Electrochem. Commun.*, 2003, **5**, 892–896.
9 S. D. Zelnick, D. R. Mattie and P. C. Stepaniak, *Aviat., Space Environ. Med.*, 2003, **74**, 1285–1291.
10 A. Serov and C. Kwak, *Appl. Catal., B*, 2010, **98**, 1–9.
11 J.-W. Mo, B. Ogorevc, X. Zhang and B. Pihlar, *Electroanalysis*, 2000, **12**, 48–54.
12 M. Strous and M. S. Jetten, *Annu. Rev. Microbiol.*, 2004, **58**, 99–117.
13 P. Ortega-Barrales, A. Molina-Díaz, M. I. Pascual-Reguera and L. F. Capitán-Vallvey, *Anal. Chim. Acta*, 1997, **353**, 115–122.
14 IARC monographs on the evaluation of carcinogenic risks to humans, 1999, **71 Pt 1**, 1–315.
15 C. A. Reilly and S. D. Aust, *Chem. Res. Toxicol.*, 1997, **10**, 328–334.
16 L. T. Ou and J. J. Street, *Bull. Environ. Contam. Toxicol.*, 1987, **38**, 179–183.
17 B. Toth, *Cancer Res.*, 1975, **35**, 3693–3697.
18 M. D. Scales and J. A. Timbrell, *J. Toxicol. Environ. Health*, 1982, **10**, 941–953.
19 C. J. Waterfield, J. A. Turton, M. D. Scales and J. A. Timbrell, *Arch. Toxicol.*, 1993, **67**, 244–254.
20 P. R. Ortiz de Montellano, O. Augusto, F. Viola and K. L. Kunze, *J. Biol. Chem.*, 1983, **258**, 8623–8629.
21 K. Bando, T. Kunimatsu, J. Sakai, J. Kimura, H. Funabashi, T. Seki, T. Bamba and E. Fukusaki, *J. Appl. Toxicol.*, 2011, **31**, 524–535.
22 G. Wang, C. Zhang, X. He, Z. Li, X. Zhang, L. Wang and B. Fang, *Electrochim. Acta*, 2010, **55**, 7204–7210.
23 G. Choudhary and H. Hansen, *Chemosphere*, 1998, **37**, 801–843.
24 X.-G. Li, R. Liu and M.-R. Huang, *Chem. Mater.*, 2005, **17**, 5411–5419.
25 H. Bhutani, S. Singh, S. Vir, K. K. Bhutani, R. Kumar, A. K. Chakraborti and K. C. Jindal, *J. Pharm. Biomed. Anal.*, 2007, **43**, 1213–1220.
26 M. Sun, L. Bai and D. Q. Liu, *J. Pharm. Biomed. Anal.*, 2009, **49**, 529–533.
27 A. Umar, M. M. Rahman, S. H. Kim and Y.-B. Hahn, *Chem. Commun.*, 2008, 166–168.
28 H. E. Malone, *Anal. Chem.*, 1961, **33**, 575–577.
29 Z. K. He, B. Fuhrmann and U. Spohn, *Anal. Chim. Acta*, 2000, **409**, 83–91.
30 E. C. Olson, *Anal. Chem.*, 1960, **32**, 1545–1547.
31 J. Liu, W. Zhou, T. You, F. Li, E. Wang and S. Dong, *Anal. Chem.*, 1996, **68**, 3350–3353.
32 Y. Y. Tang, C. L. Kao and P. Y. Chen, *Anal. Chim. Acta*, 2012, **711**, 32–39.
33 J. R. Stetter, K. F. Blurton, A. M. Valentine and K. A. Tellefsen, *J. Electrochem. Soc.*, 1978, **125**, 1804–1807.
34 X. Gu and J. P. Camden, *Anal. Chem.*, 2015, **87**, 6460–6464.
35 X.-Y. Zhang, Y.-S. Yang, W. Wang, Q.-C. Jiao and H.-L. Zhu, *Coord. Chem. Rev.*, 2020, **417**, 213367.
36 N. Vijay and S. Velmathi, *ACS Sustainable Chem. Eng.*, 2020, **8**, 4457–4463.
37 X. Yang, Y. Liu, Y. Wu, X. Ren, D. Zhang and Y. Ye, *Sens. Actuators, B*, 2017, **253**, 488–494.
38 Y. He, Z. Li, B. Shi, Z. An, M. Yu, L. Wei and Z. Ni, *RSC Adv.*, 2017, **7**, 25634–25639.
39 T. Tang, Y.-Q. Chen, B.-S. Fu, Z.-Y. He, H. Xiao, F. Wu, J.-Q. Wang, S.-R. Wang and X. Zhou, *Chin. Chem. Lett.*, 2016, **27**, 540–544.
40 S. K. Manna, A. Gangopadhyay, K. Maiti, S. Mondal and A. K. Mahapatra, *ChemistrySelect*, 2019, **4**, 7219–7245.
41 B. Roy and S. Bandyopadhyay, *Anal. Methods*, 2018, **10**, 1117–1139.
42 S. K. Samanta, K. Maiti, S. S. Ali, U. N. Guria, A. Ghosh, P. Datta and A. K. Mahapatra, *Dyes Pigm.*, 2020, **173**, 107997.
43 Z. Li, W. Zhang, C. Liu, M. Yu, H. Zhang, L. Guo and L. Wei, *Sens. Actuators, B*, 2017, **241**, 665–671.
44 Y. Ban, R. Wang, Y. Li, Z. An, M. Yu, C. Fang, L. Wei and Z. Li, *New J. Chem.*, 2018, **42**, 2030–2035.
45 J. Du, X. Li, S. Ruan, Y. Li, F. Ren, Y. Cao, X. Wang, Y. Zhang, S. Wu and J. Li, *Analyst*, 2020, **145**, 636–642.
46 D. Bu, Y. Wang, N. Wu, W. Feng, D. Wei, Z. Li and M. Yu, *Chin. Chem. Lett.*, 2021, **32**, 1799–1802.
47 S. Wang, S. Ma, J. Zhang, M. She, P. Liu, S. Zhang and J. Li, *Sens. Actuators, B*, 2018, **261**, 418–424.